Supporting Information

Topotactic Transformation of Zeolitic Imidazolate Framework into High-Performance Battery Type Electrode for Supercapattery Application

Jatin Sharma[†], *Srinivasan Alagar*[†], *Aashi, Rajdeep Kaur, Ashish Gaur, Krishankant, Vikas Pundir, Deepak Upreti, Rekha Rani, Arun K, Vivek Bagchi**

Institute of Nano Science and Technology, Sector-81, Knowledge City, Sahibzada Ajit Singh Nagar, Punjab, 140306, INDIA

†Both authors contributed equally

**Corresponding Author*

Dr. Vivek Bagchi

Email: vivekbagchi@gmail.com, bagchiv@inst.ac.in

S1. Materials characterization

The synthesized materials were analyzed by using X-ray diffraction (PXRD, Bruker-D8 advance) with Cu Ka radiation (1.5406 Å) at 40 kV/25 mA at a scan rate $0.06°s^{-1}$ with a 2θ angle from 5 to 60. The samples' morphologies were obtained from SEM (SEM, Hitachi SU8010) and TEM (HR-TEM, Tecnai G2). The XPS spectra were obtained by using a PHI spectrometer (Perkin-Elmer, America) with monochromatic Mg radiation (hν=1253.6 eV). The surface area of the catalyst was determined by performing a Brunauer-Emmet-Teller (BET) analysis. This analysis was conducted using an Autosorb IQ Quantachrome instrument.

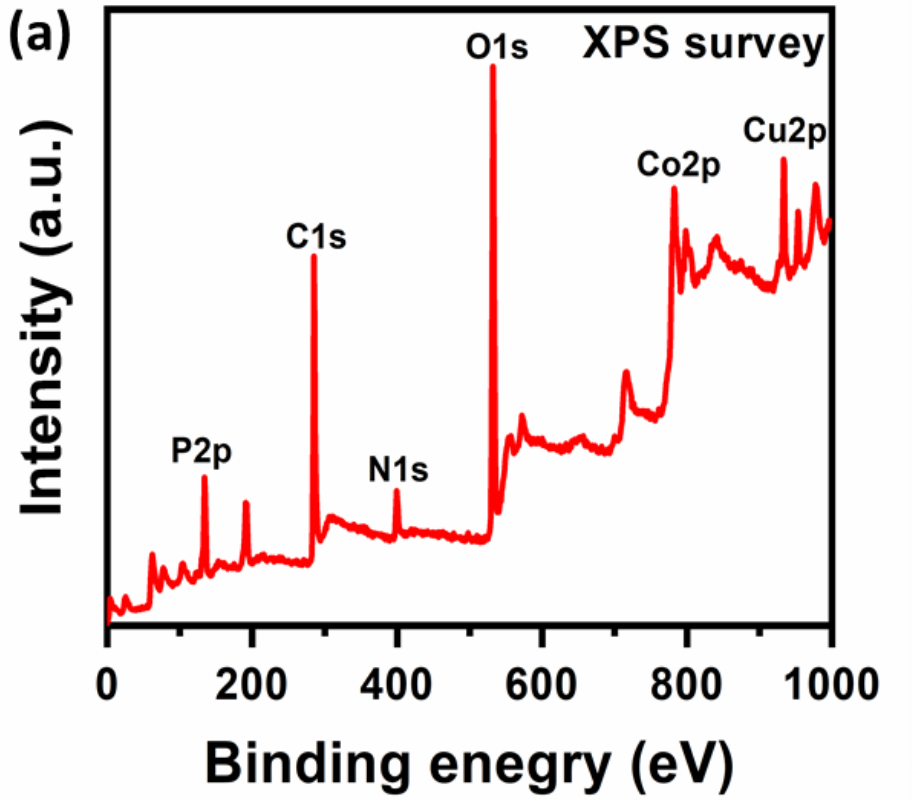

Figure S1. XPS survey spectra of CCP-5-NPC

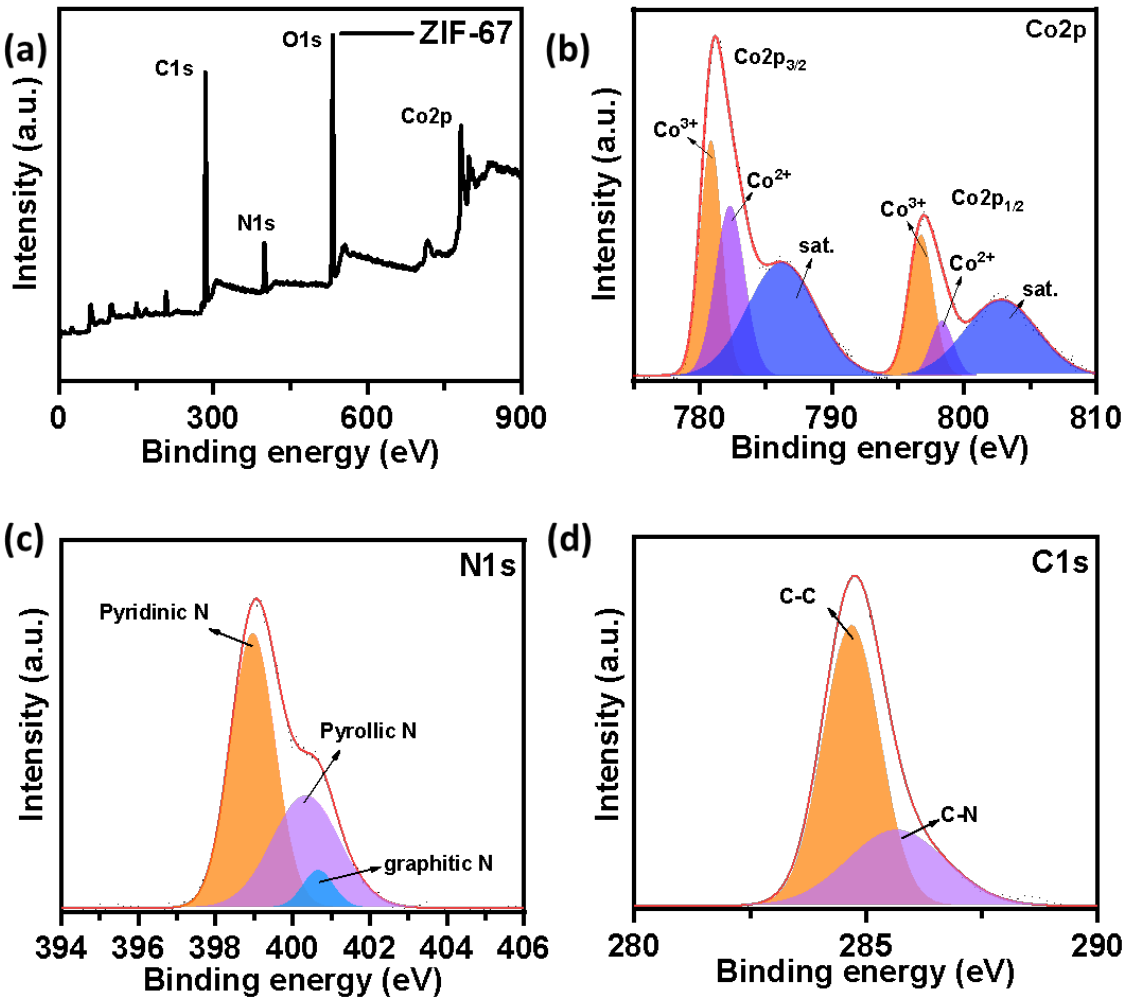

Figure S2. XPS survey of ZIF-67 (b) Co, (c) N, (d) C

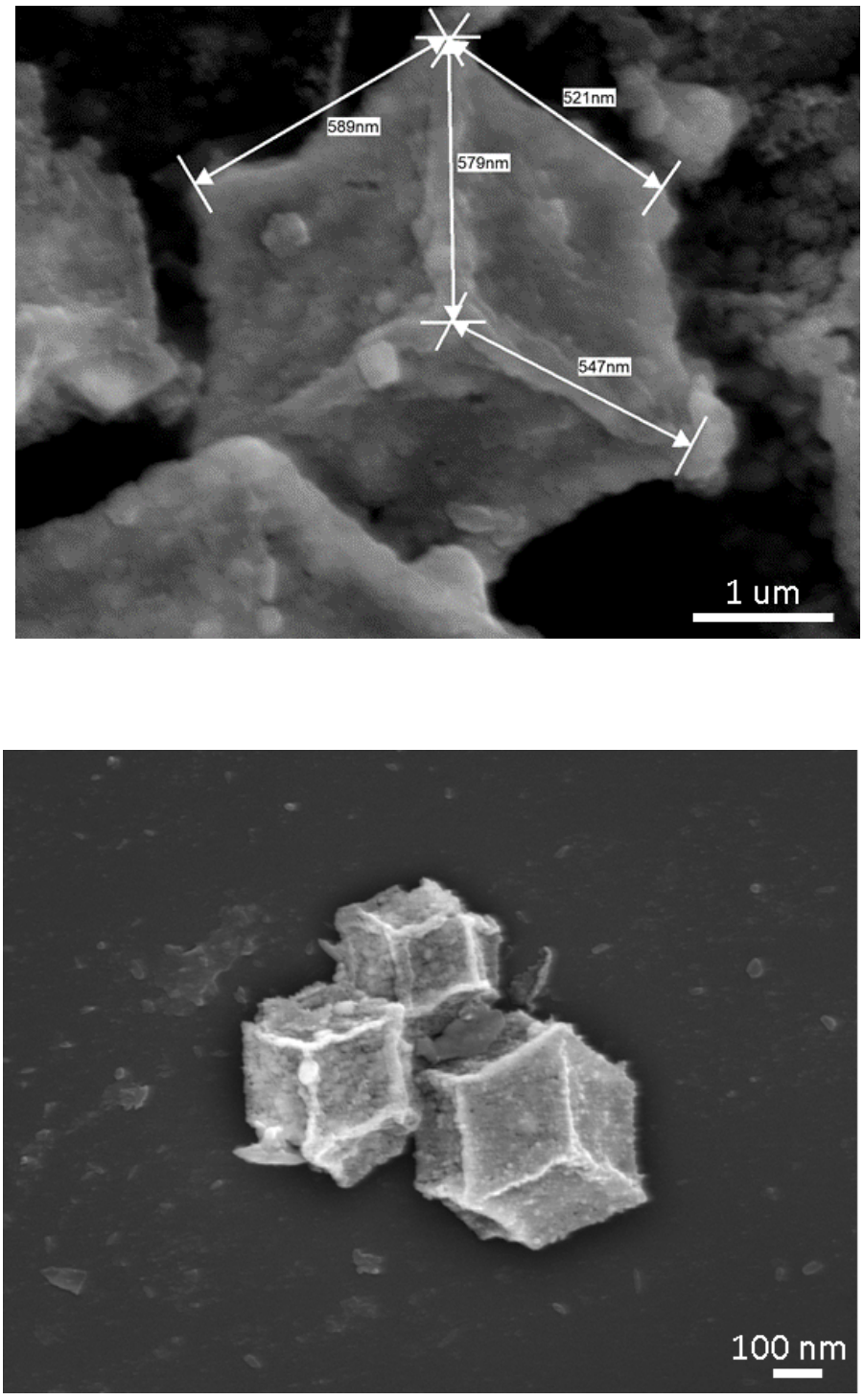

Figure S3. FESEM image of CCP-3-NPC

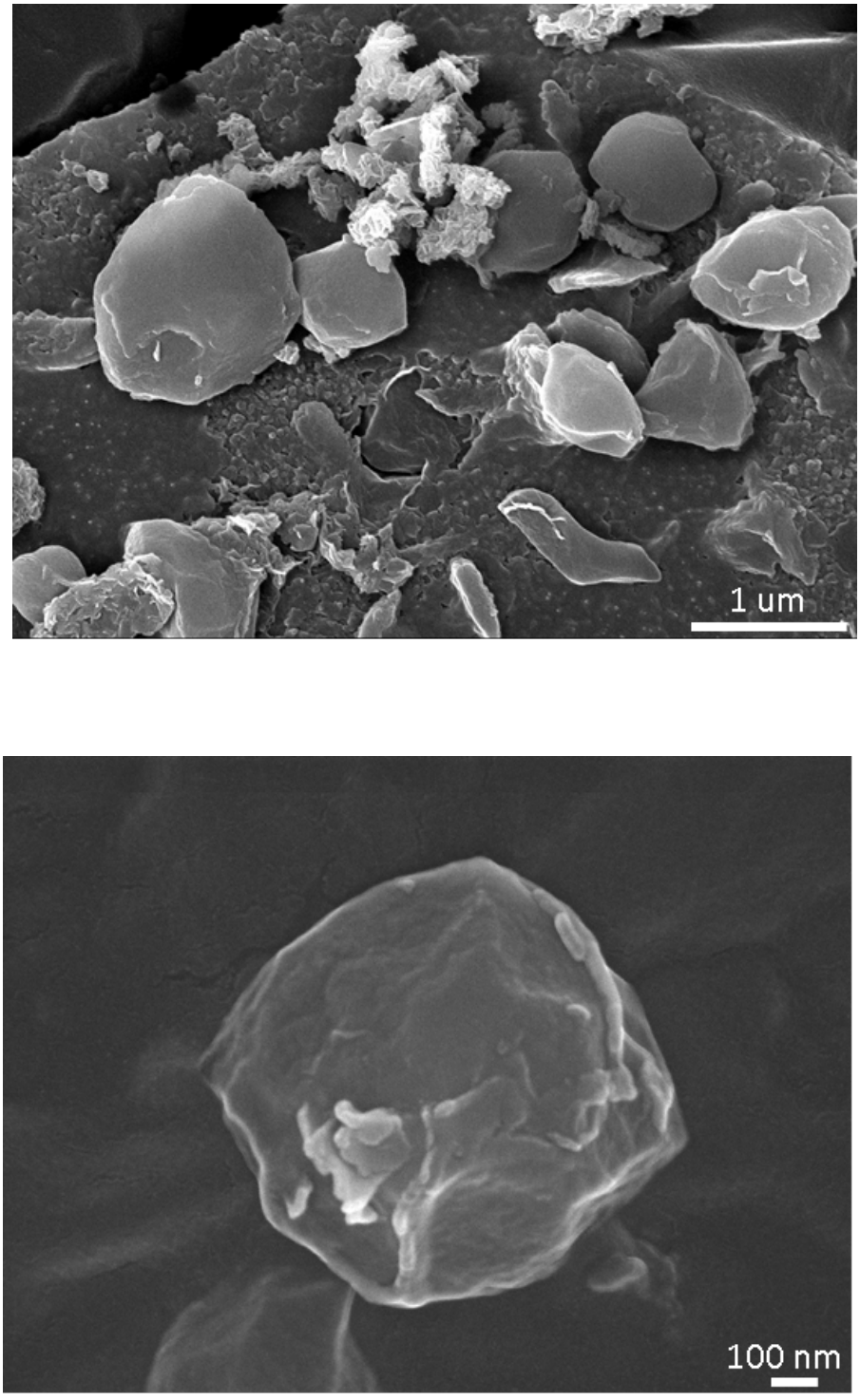

Figure S4. FESEM image of SEM CCP-7-NPC

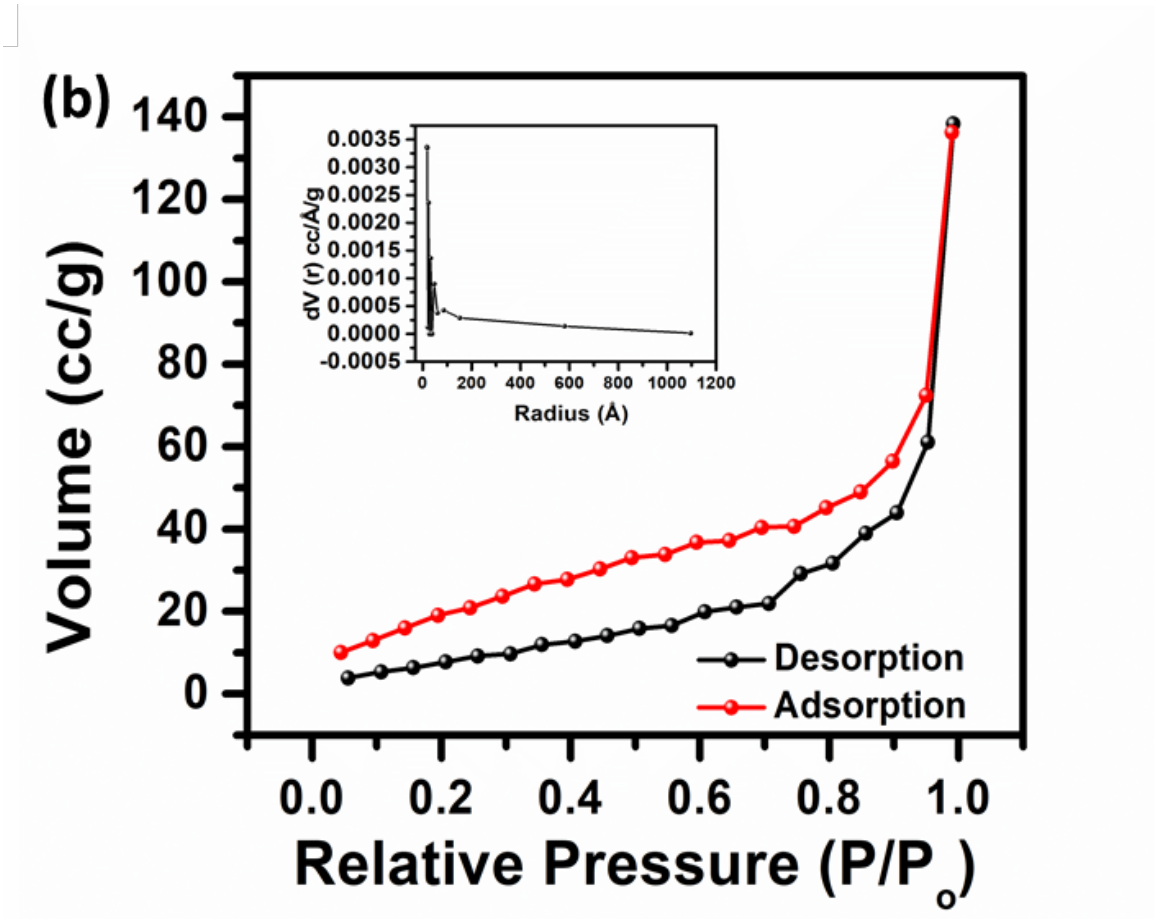

Figure S5. BET data of CCP-5-NPC

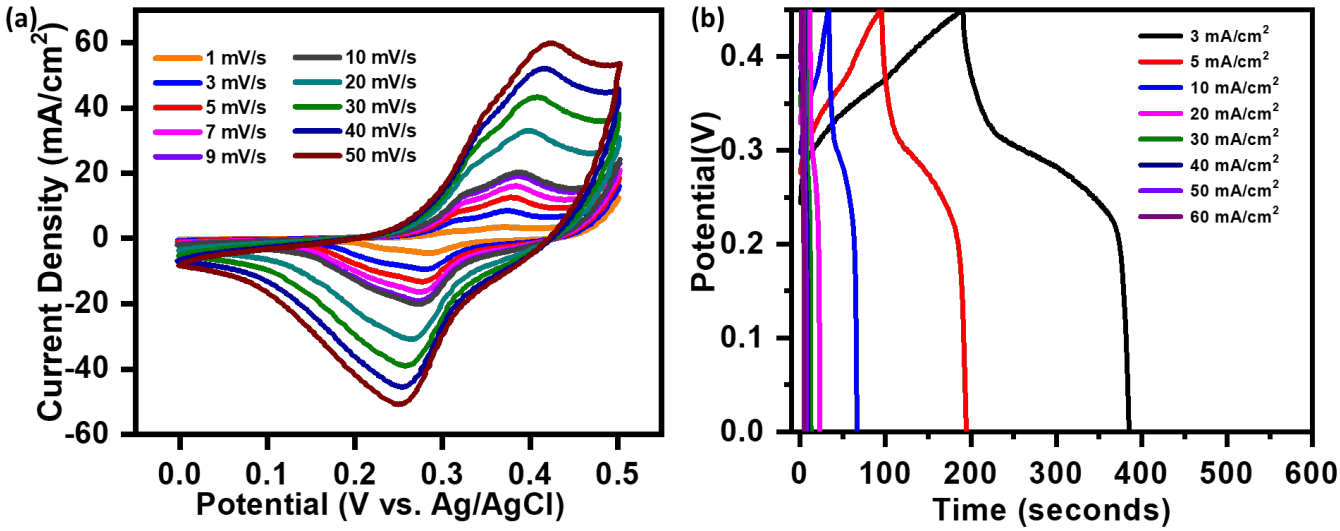

Figure S6. ZIF-67 electrochemical data (a) CV at various scan rates (b) GCD at various current densities

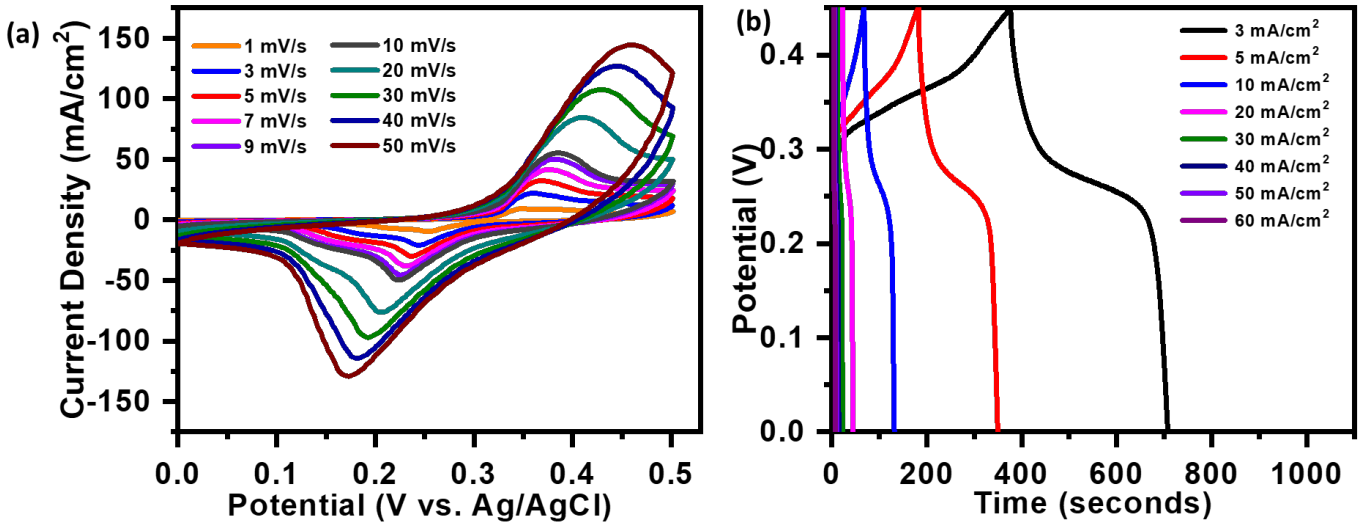

Figure S7. Cobalt Oxide electrochemical data (a) CV at various scan rates (b) GCD at various current densities

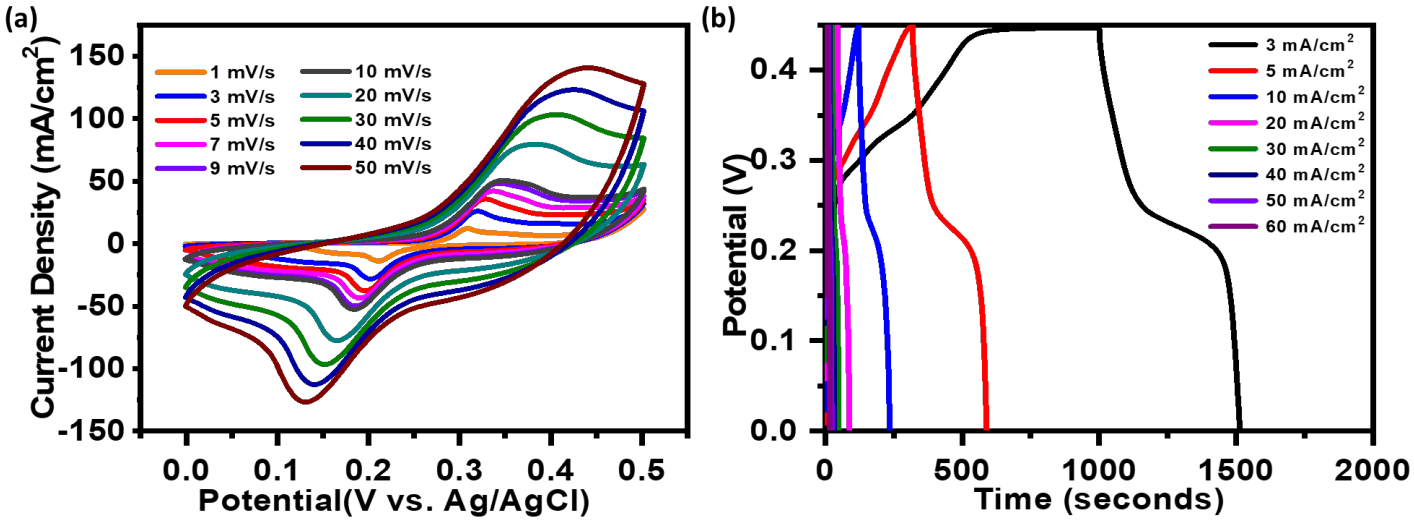

Figure S8. CoP-NC Electrochemical data (a) CV at various scan rates (b) GCD at various current density

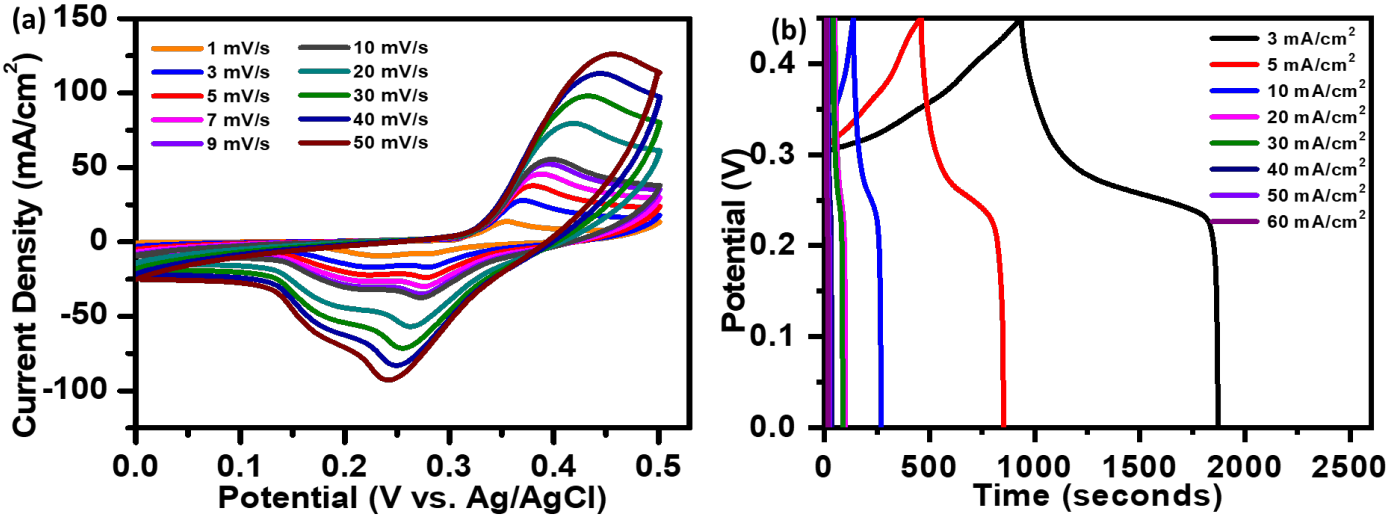

Figure S9. CCP-3-NPC Electrochemical data (a) CV at various scan rates (b) GCD at various current density

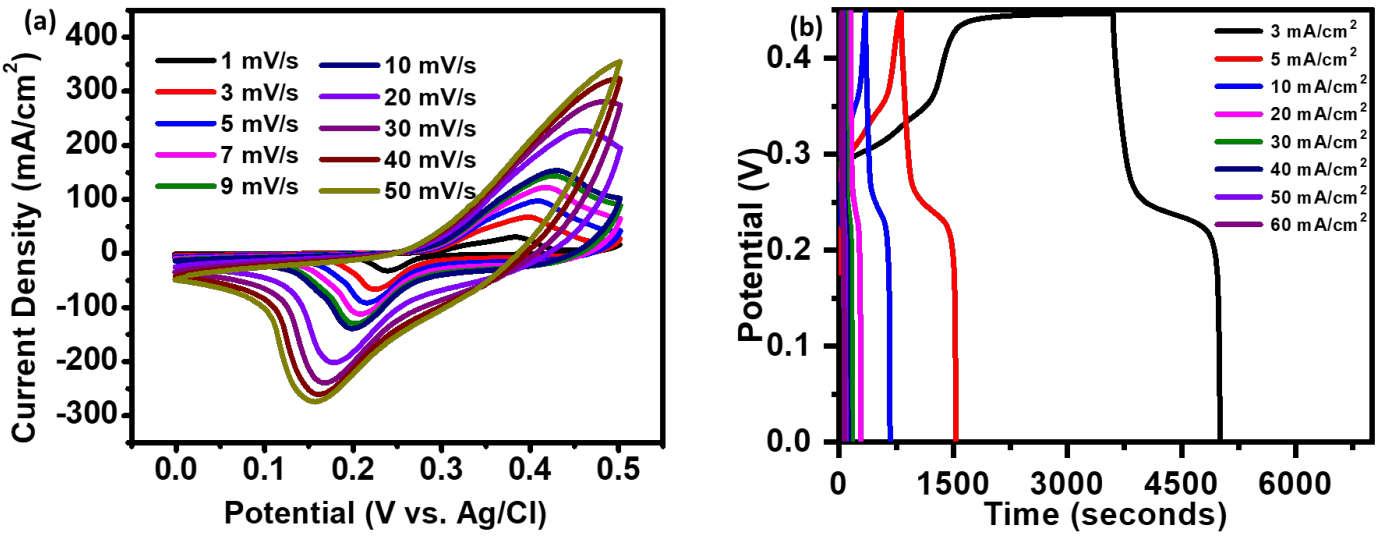

Figure S10. CCP-5-NPC Electrochemical data (a) CV at various scan rates (b) GCD at various current density

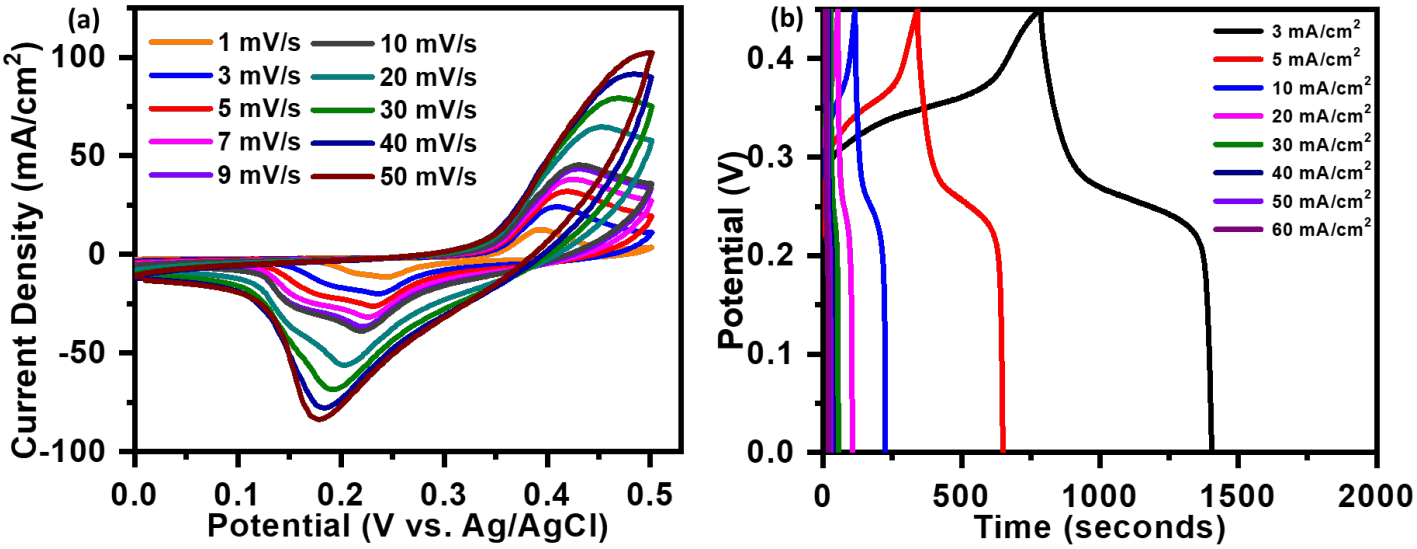

Figure S11. CCP-7-NPC Electrochemical data (a) CV at various scan rates (b) GCD at various current density

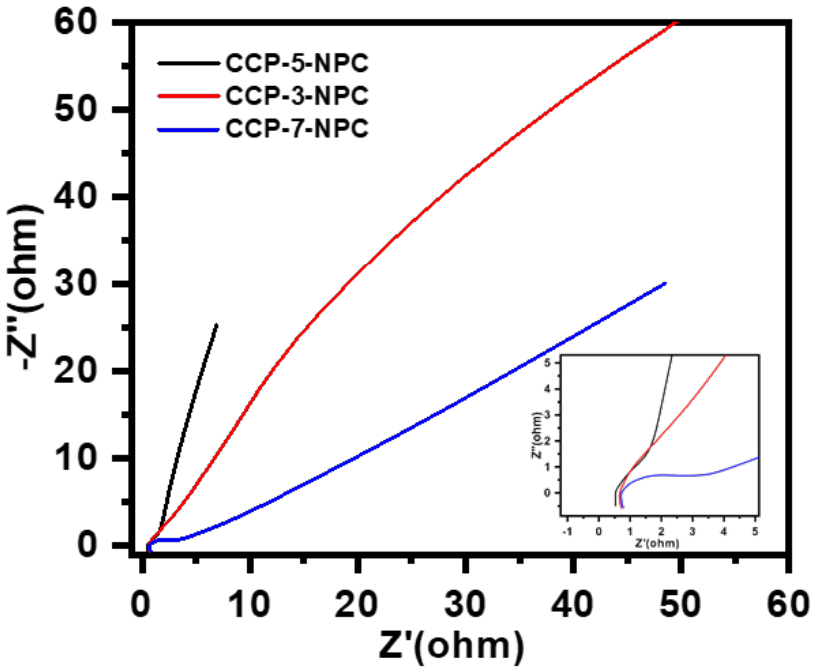

Figure S12. EIS comparison of CCP-5-NPC (x = 3,5,7)

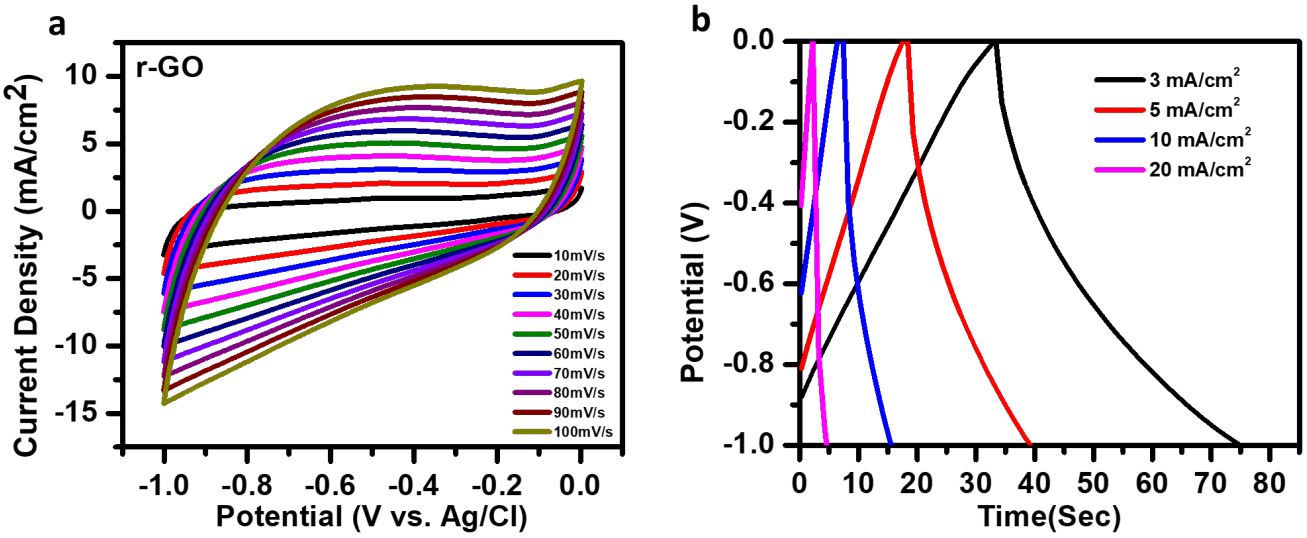

Figure S13. Electrochemical performance of r-GO a) CV plot, b) GCD plot

In Figure S13 a, a CV measurement was done to check the electrochemical performance of the r-GO at different scan rates from the potential window of 0 to -1 V. Similarly, a GCD was performed to evaluate the charge-discharge time at different current densities from a potential window of 0 to -1 V. The capacitance value was calculated using the GCD, and it was noticed that it exhibited a capacitance of 0.278 F/cm^2 at 3 mA/cm^2.

S. no.	Current density (mA/cm^2) / Materials	Capacitance (F/cm^2)						
		ZIF-67	Co_xP_y	CoP-NC	CCP-1-NPC	CCP-3-NPC	**CCP-5-NPC**	CCP-7-NPC
1	3	0.83	1.41	2.19	2.29	3.99	**5.99**	2.63
2	5	0.71	1.19	1.93	2.07	2.79	**5.13**	2.20
3	10	0.47	0.91	1.62	1.39	1.89	**4.61**	1.56
4	20	0.34	0.62	1.22	0.93	1.39	**3.98**	1.48
5	30	0.30	0.47	1.02	0.68	0.98	**3.584**	1.19
6	40	0.28	0.45	0.88	0.53	0.97	**3.18**	1.02
8	50	0.28	0.35	0.79	0.39	0.85	**2.92**	0.92
9	60	0.26	0.34	0.72	0.25	0.768	**2.73**	0.77

Table S1. Specific Capacitance of all electrodes in three-electrode system calculated arealy.

Electrode Material	Capacitance	Electrolyte	Potential Window	Stability	Retention
CCP-5-NPC (This Work)	**5.99 F/cm^2 at 3 mA/cm^2**	**1M KOH**	**0 to 0.5 V**	**10,000**	**87%**
CoMNS@CoP/NF [1]	886.8 μA h/cm^2 at 5 mA/cm^2	1M KOH	-0.1 to 0.5 V	10,000	87.4%
CoPN/NF [2]	1.57 mAh/ cm^2 at 2 mA/cm^2	6M KOH	0 to 0.5 V	5000	71%
$NiCo_2O_4$[3]	281.7 F cm^{-3} at 96.8 mA cm^{-3}	3M KOH	0 to 0.5 V		
MNPC-0.5/NF [4]	4461 mC/ cm^2 at 2 mA/ cm^2	1M KOH	0 to 0.5 V	5000	83%
CoP nanowire [5]	513 mF/ cm^2 at 1 mA/ cm^2	1 M LiCl aqueous solution	0 to -0.8 V	5000	87.05%
Co_3O_4@Co–CH[6]	1.324 F/ cm^2 at 3 mA/ cm^2	2M KOH	0 to 0.5 V	5000	72.1%
Co-MOF/NCS [7]	1.59 F/ cm^2 at 1 mA/ cm^2	2M KOH	0 to 0.5 V	10,000	89.58%
Ni–CoP_3/NF[8]	5.1 F/ cm^2 at 2.5 mA/ cm^2	6M KOH	0 to 0.5 V	10,000	90.2%
Mn–CoP/NF[9]	6.84 F/ cm^2 at 5 mA/ cm^2	6M KOH	0 to 0.5 V	2000	82.1%
Co-MOF/NF(1200)[10]	1.53 F/ cm^2 at 1 mA/ cm^2	1 M LiOH aqueous	0 to 0.5 V	10,000	71%

Table S2. Areal capacitance comparison table of different electrode related to CCP-5-NPC

Electrode Material	Capacitance	Electrolyte	Energy Density	Power Density	Potential Window (V)	Stability (Cycles)	Retention
CCP-5-NPC || r-GO (This work)	1.8 F/ cm^2 at 3 mA/ cm^2	**6M KOH**	**0.56 mWh/cm^2**	**4.89 mW/cm^2**	0 to 1.5 V	**10,000**	**87.7 %**
CoM NS@CoP-6 h/NF//AC/NF [1]	1.554 F/ cm^2 at 5 mA/cm^2	1M KOH	0.44 mWh/cm^2	3.48 mW/cm^2	0 to 1.5 V	10,000	85.2%
CoPN/NF//PCP/NF [2]	3.81 F/cm^2 at 5 mA/cm^2	6M KOH	0.75 mWh/cm^2	77.53 mW/cm^2	0 to 1.5 V	5000	80%
CNT@$NiCo_2O_4$ // CNT@$NiCo_2O_4$ [3]	23.3 F cm^{-3} at 80.6 mA cm^{-3}	PVA+ KOH	3.2 mWh cm^{-3}	18.5 mW cm^{-3}	0 to 1 V	5000	95.6%
MNPC-0.5/NF//GH/NF [4]		PVA + KOH	1.8 mWh cm^{-3}	750 mW cm^{-3}	0 to 1.5 V	5000	87%
CoP//MnO_2 [5]	1.94 F/cm^3 at 1 mA/cm^2	1 M LiCl aqueous solution	0.69 mWh cm^{-3}	10.15 mW cm^{-3}	0 to 1.6 V	5000	82%
Co_3O_4@Co–CH//KOH//AC/NF [6]	87 mF/cm^2 At 3 mA/cm^2	PVA/KOH	0.025 mWh/cm^2	3.371 mW/cm^2	0 to 1.5 V	10,000	97.3%
Co-MOF/NCS//AC [7]	0.605 F/ cm^2 at 3 mA/ cm^2	2M KOH	0.215 mW/cm^2	1.778 mW/cm^2	0 to 1.6 V	10,000	88%

Co-MOF@NiCo-LDH//AC[11]	2.84 F/ cm^2 at 10 mA/ cm^2	2M KOH	0.89 mWh/cm^2	7.5 mW/cm^2	0 to 1.5 V	10,000	97.6%
Co-MOF/NF//AC ASC[10]	671 mF/ cm^2 at 5 mA/ cm^2	PVA/LiOH	210 $\mu Wh/cm^2$	3761.2 $\mu W/cm^2$	0 to 1.5 V	10,000	74%

Table S3. Areal capacitance comparison table of different electrode related to CCP-5-NPC || r-GO device

Current Density	Capacitance F/cm^3	Energy Density Wh/cm^3	Power Density W/cm^3
3	9.000806	5.625504	48.96
5	7.221419	4.513387	81.6
10	4.251904	2.65744	163.2
20	1.821167	1.138229	326.4
30	0.887589	0.554743	489
40	0.623206	0.389504	652.8
50	0.487279	0.304549	816

Table S4. Electrochemical evaluation of the device done volumetrically.

The device shows the volumetric capacitance, energy density, and power density of 9.0 F/cm^3, 5.62 mWh/cm^3 and 48.96 mW/cm^3 at 3mA/cm^3.

S2: electrochemical mechanism:

In a KOH electrolyte, a Cu-doped CoP electrode undergoes complex electrochemical reactions where both Cu and Co participate in redox processes. The adsorption and desorption of ions during electrochemical occurs with the reversible interconversion of Cu^+/Cu^{2+} and Co^{2+}/Co^{3+}. The following chemical equations may be used to explain the reversible oxidation-reduction reaction mechanism of Cu-CoP/NPC.[12]

$$Cu - CoP + OH^- \leftrightarrow CuOH + CoPOH + e^-$$

$$CuOH + OH^- \leftrightarrow CuO + H_2O + e^-$$

$$CoPOH + OH^- \leftrightarrow CoO + H_2O + e^-$$

Cu doping improves electrochemical reversibility, decreases CoP polarization, and raises total electrical conductivity. Additionally, as can be seen in supporting data figure S12, 5% Cu doping results in the lowest Rct, which facilitates quicker ion and electron movement in the interface during an electrochemical reaction.

S3. References

(1) Yu, Y.; Han, Y.; Cui, J.; Wang, C. A Cobalt-Based Metal–Organic Framework Electrodeposited on Nickel Foam as a Binder-Free Electrode for High-Performance Supercapacitors. New J. Chem. 2022, 46 (26), 12565–12571. https://doi.org/10.1039/D2NJ01870E

(2) Elshahawy, A. M.; Guan, C.; Zang, W.; Ding, S.; Kou, Z.; Pennycook, S. J.; Yan, N.; Wang, J. Phospho-Oxynitride Layer Protected Cobalt Phosphonitride Nanowire Arrays for High-Rate and Stable Supercapacitors. *ACS Appl. Energy Mater.* **2019**, *2* (1), 616–626. https://doi.org/10.1021/acsaem.8b01645.

(3) Hu, Y.; Wang, Q.; Chen, S.; Xu, Z.; Miao, M.; Zhang, D. Flexible Supercapacitors Fabricated by Growing Porous NiCo2O4 In Situ on a Carbon Nanotube Film Using a Hyperbranched Polymer Template. *ACS Appl. Energy Mater.* **2020**, *3* (4), 4043–4050. https://doi.org/10.1021/acsaem.0c00491.

(4) Wang, S.; Zhang, D.; Meng, H.; Cao, S.; Zhang, L. Mg-Doped NiCoP Microflower Grown on Ni Foam for High-Capacity Supercapacitor Electrode. *Eur. Phys. J. Appl. Phys.* **2023**, *98*, 24. https://doi.org/10.1051/epjap/2023220329.

(5) Zheng, Z.; Retana, M.; Hu, X.; Luna, R.; Ikuhara, Y. H.; Zhou, W. Three-Dimensional Cobalt Phosphide Nanowire Arrays as Negative Electrode Material for Flexible Solid-State

Asymmetric Supercapacitors. *ACS Appl. Mater. Interfaces* **2017**, *9* (20), 16986–16994. https://doi.org/10.1021/acsami.7b01109.

(6) Sheng, P.; Tao, S.; Gao, X.; Tan, Y.; Wu, D.; Qian, B.; Chu, P. K. Design and Synthesis of Dendritic Co3O4@Co2(CO3)(OH)2 Nanoarrays on Carbon Cloth for High-Performance Supercapacitors. *J Mater Sci* **2020**, *55* (26), 12091–12102. https://doi.org/10.1007/s10853-020-04819-9.

(7) Velhal, N. B.; Maile, N. C.; Paeng, C.; Lee, H.; Kim, T.; Kim, J.; Yim, C. Cobalt-Based Metal-Organic Framework/Nickel-Cobalt Sulphide Composite Nanopetal Arrays for High-Performance Hybrid Coin Cell Supercapacitor. *Journal of Energy Storage* **2024**, *90*, 111764. https://doi.org/10.1016/j.est.2024.111764.

(8) Jiang, J.; Li, Z.; He, X.; Hu, Y.; Li, F.; Huang, P.; Wang, C. Novel Skutterudite CoP3–Based Asymmetric Supercapacitor with Super High Energy Density. *Small* **2020**, *16* (31), 2000180. https://doi.org/10.1002/smll.202000180.

(9) Zhu, G.; Yang, L.; Wang, W.; Ma, M.; Zhang, J.; Wen, H.; Zheng, D.; Yao, Y. Hierarchical Three-Dimensional Manganese Doped Cobalt Phosphide Nanowire Decorated Nanosheet Cluster Arrays for High-Performance Electrochemical Pseudocapacitor Electrodes. *Chemical Communications* **2018**, *54* (66), 9234–9237. https://doi.org/10.1039/C8CC02475H.

(10) Yu, Y.; Han, Y.; Cui, J.; Wang, C. A Cobalt-Based Metal–Organic Framework Electrodeposited on Nickel Foam as a Binder-Free Electrode for High-Performance Supercapacitors. *New J. Chem.* **2022**, *46* (26), 12565–12571. https://doi.org/10.1039/D2NJ01870E.

(11) Ye, F.; Zhou, J.-J.; Jiang, X.; Wang, L.; Su, Y.; Zhu, B.; Chen, L. Hierarchical Columnar Cactus-like Co-MOF@NiCo-LDH Core–Shell Nanowrinkled Pillar Arrays for Supercapacitors with Ultrahigh Areal Capacitance. *ACS Appl. Energy Mater.* **2023**, *6* (9), 4844–4853. https://doi.org/10.1021/acsaem.3c00341.

(12) Zhu, L.; Ye, S.; Zhu, X.; Wang, Y.; Tang, Y.; Pan, Y.; Meng, Z.; Oh, W.; Fan, L.; Zhang, Q. Phosphorization Engineering of CoP/NiCoP Nanoneedle Arrays for Energy Storage. *ACS Appl. Nano Mater.* **2024**, *7* (14), 16097–16107. https://doi.org/10.1021/acsanm.4c01981.